

Numerical modeling for trapped-ion thermometry using dark resonances

Muriel Bonetto,^{1,2} Nicolás Adrián Nuñez Barreto,^{1,2} Christian Tomás Schmiegelow,^{1,2} and Cecilia Cormick^{3,4}

¹Universidad de Buenos Aires, Facultad de Ciencias Exactas y Naturales,
Departamento de Física, Laboratorio de Iones y Átomos Fríos,
Pabellón 1, Ciudad Universitaria, 1428 Buenos Aires, Argentina

²CONICET - Universidad de Buenos Aires, Instituto de Física de Buenos Aires (IFIBA),
Pabellón 1, Ciudad Universitaria, 1428 Buenos Aires, Argentina

³Universidad de la República, Facultad de Ingeniería, Instituto de Física,
Julio Herrera y Reissig 565, 11300 Montevideo, Uruguay

⁴Instituto de Física Enrique Gaviola, CONICET and Universidad Nacional de Córdoba,
Ciudad Universitaria, X5016LAE, Córdoba, Argentina

(Dated: May 12, 2025)

The accurate simulation of vibrational energy transport and quantum thermodynamics with trapped ions requires good methods for the estimation of temperatures. One valuable tool with this purpose is based on the fit of dark resonances in the fluorescence spectrum. However, the reliability of the procedure is still unclear. Here, we discuss several techniques with simplified dynamical equations for the numerical simulation of the spectrum of a trapped ion undergoing thermal motion, identifying advantages and limitations of each method. We start with a simplified three-level model to provide a better insight into the approximations involved and then move on to tackle the experimentally relevant case of an eight-level calcium ion. We observe that mimicking the effect of thermal motion by means of additional dephasing is computationally very convenient but can lead to significant errors in the estimation of the temperature. However, this can be counteracted by a proper calibration, supporting the use of dark resonances as a practical thermometer.

I. INTRODUCTION

Trapped ions constitute a versatile platform for exploring thermodynamic processes at the microscopic scale. Their ability to form various crystalline structures, such as linear chains, zigzag configurations, or more complex geometries, makes them ideal for investigating heat transport [1–5], out-of-equilibrium thermodynamics [6–8], and thermal engines [9, 10]. For example, by tuning the coupling between ions, these systems can exhibit transitions between ballistic and diffusive transport regimes [1, 3], offering valuable insights into the emergence of macroscopic thermodynamic behavior, such as Fourier’s law, at microscopic scales. The exploration of such phenomena requires accurate thermometry of each trapped ion.

For an ergodic and fully thermalized system, temperature is a measure of the mean kinetic energy. However, in trapped ion systems, the kinetic energy may vary across different degrees of freedom, leading to direction-dependent effective temperatures, which occurs due to an nonexistent, or low, coupling of these variables. Furthermore, temperature measurements typically rely on ensemble averages, but in trapped ion systems measurements are often performed over multiple trials of the same system in interaction with its environment.

Several methods have been developed for temperature determination in trapped ions. For temperatures above a few Kelvin, spatial spreading of the ions can be used effectively [11–14]. For lower temperatures, in the sub Kelvin range, Doppler broadening of spectral lines offers temperature estimates constrained by the linewidth of the selected transition, which typically lies in the 10 MHz

range for dipole-allowed transitions [15–17]. For even lower temperatures, in the micro-Kelvin range, sharper spectral features, such as motional sidebands observed in quadrupole transitions or Raman spectroscopy, with linewidths typically in the Hertz range, enable precise measurements of the thermal population of a given motion mode, but do not directly measure the mean kinetic energy of a given atom/ion [18–21].

A particularly promising ion thermometry approach involves the use of Coherent Population Trapping (CPT), also known as Dark Resonance spectroscopy [22–24]. This method, which relies on a two-photon process, leverages narrow spectral lines to measure temperatures from a few milli-Kelvin down to the micro-Kelvin range.

Fluorescence spectra displaying so-called “dark resonances” have been shown to provide a path for the characterization of thermal motion in this regime. These dark resonances are sharp reductions in fluorescence due to partial coherent population trapping (CPT) between different atomic sublevels. As thermal motion leads to a Doppler shift of the laser fields, thermal effects lead to a broadening and blurring of the resonances, so that CPT spectra can constitute useful thermometers. More precisely, from a fit of the depth and width of such spectral features one can obtain estimations of the temperature.

Although powerful, a precise temperature measurement from a CPT spectrum requires computationally intensive fits of experimental data to theoretical spectra. As a full simulation of the coupled dynamics of all electronic levels and motional states is too costly to be practical, alternative, more economical approximations are convenient. As we show in this paper, while these approximations make calculations more manageable, they

also introduce errors, causing different numerical methods to yield varying results.

In this work, we analyze and compare various approximation techniques that can be used to determine the temperature from a CPT spectrum. In doing so, we determine the quality and regime of applicability of different methods in their ability to model the effect of thermal motion and to extract reliable temperatures from CPT spectra in an accurate and economical fashion, and provide practical recipes for calibration and use of these methods.

For simplicity, we focus on the case of a single trapped ion. We consider the following approaches, which are detailed in section III, A) the “driven motion approximation” where we do a numerical simulation of the electronic evolution with a time-dependent Doppler shift and neglect back action of the electronic state on the motion, B) the “instantaneous relaxation approximation”, which assumes that the time scale associated with the electronic relaxation is negligible with respect to the motional dynamics, so the electronic state is calculated as the asymptotic internal state corresponding to the instantaneous velocity; C) the “sidebands approximation”, where the internal state is assumed to be periodic and the coupled equations for the different Fourier/Floquet components are solved; D) the “effective dephasing approximation”, in which the thermal broadening of the spectral lines is introduced as an additional dephasing mechanism. Each of these methods has advantages and problems and each has a certain regime of applicability, which we will discuss in detail.

As a benchmark we will use the direct numerical simulation of the electronic dynamics driven by the atomic motion. This is, we will consider that the effective detuning oscillates at the trap frequency and numerically integrate the time evolution of the optical equations until the system reaches the stationary state. By taking a temporal average of the excited state population, we estimate the fluorescence of the ion. This approach assumes that the motional degrees of freedom are not affected by the interaction with the lasers, a good approximation once the ions reach thermal equilibrium at temperatures above the Doppler limit. Within this approximation, all relevant dynamics are captured by the model. However, the resulting calculation is too demanding to be practical for spectral fits; instead, it can be used to “calibrate” the computationally more affordable methods.

We will assume that the motional state is thermal and can be described semiclassically. The exploration of non-thermal and quantum-mechanical regimes of the motion is beyond the scope of the present analysis.

For definiteness, we will focus our calculations on the case of a trapped calcium ion, where the Λ -type 3-level system, on which one observes the dark resonances is formed between states $S_{1/2} \leftrightarrow P_{1/2} \leftrightarrow D_{3/2}$ (ground-excited-metastable) connected by a 397 nm laser connecting the $S_{1/2} \leftrightarrow P_{1/2}$ and a 866 nm laser connecting the $D_{3/2} \leftrightarrow P_{1/2}$. Spectra are obtained by scanning the

detuning of the 866 nm laser while keeping the 397 nm laser at a fixed red-detuning of roughly half a linewidth. The expected fluorescence is calculated as the probability to be in one of the excited states. Naturally, the ideas presented here are not restricted to this system and can be applied to other atomic species or laser configurations that exhibits a Λ -type structure.

The work is organized as follows: In Section II we will briefly describe our model for the thermal motion of a trapped ion, and introduce the basic concepts regarding temperature estimation based on dark-resonance spectra. In Section III, we will first address the simpler case of a three-level system, to then proceed to the experimentally relevant case of the full 8-level system corresponding to trapped calcium in Section IV. Finally, in Section V we will summarize our results.

II. THERMOMETRY BASED ON DARK-RESONANCE SPECTRA

A. Dark resonances

Our atomic system of interest is such that the relevant electronic levels can be described as a Λ -type structure, as shown in Fig. 1. For simplicity, here we will restrict to only three levels. Realistic models with more levels display similar phenomena, as will be discussed in Section IV. Here, we will assume that levels $|0\rangle$ and $|2\rangle$ are stable and have dipole-allowed transitions to an excited level $|1\rangle$, from which the atom can spontaneously decay back to the stable states. Each transition is driven with a Rabi frequency $\Omega_{0/2}$ and a detuning $\Delta_{0/2}$ from the top level.

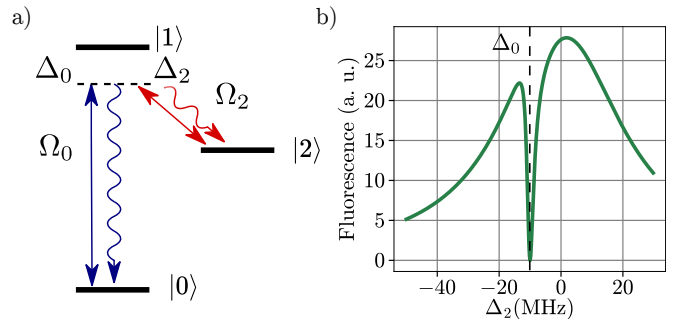


FIG. 1: a) Schematic representation of a three-level atom in a lambda configuration. Ω_0 and Ω_2 are the Rabi frequencies of the transitions while Δ_0 and Δ_2 the detunings of the respective lasers. b) Example of the CPT spectra for a three level system.

If atomic motion is neglected and the laser detunings are equal, there is a coherent superposition of levels $|0\rangle$ and $|2\rangle$ that does not couple to the light field. Spontaneous decay eventually takes the atomic population to this combination, and the state remains unchanged by the laser drive and the atom stops fluorescing. This coherent superposition is then called a “dark state” and

the phenomenon is referred to as “coherent population trapping” (CPT). In terms of the atomic spectra, when one of the laser fields has a fixed frequency but the other frequency is varied, the presence of a dark state manifests as an abrupt decay in atomic fluorescence, as shown in Fig. 1 (b). This kind of measurement is called a “CPT spectrum” and the decay in emission is a “dark resonance”. For an atom at rest, the width and depth of these spectral features are determined by the laser linewidth, atomic linewidth, and intensity of the lasers used. When the laser fields are such that the motion induces a different Doppler shift $\Delta_{0/2}$ for each transition, the resonances also depend on the velocity v of the ion, since

$$\delta_0 - \delta_2 = \Delta_0 - \Delta_2 - (\vec{k}_0 - \vec{k}_2) \cdot \vec{v}. \quad (1)$$

The fact that dark resonances are sensitive to motion makes CPT spectra a useful resource for atomic thermometry, as will be explained in the following.

B. Semiclassical model for the thermal motion of a trapped ion

We will consider a single ion trapped in a radiofrequency trap. Under typical operation conditions, the motion of the ion can be split into two components: a fast oscillation with small amplitude at the frequency of the trapping field, and a slower motion with larger amplitude that can be described as oscillation in an effective static harmonic potential or “pseudopotential”. The former is usually called “micromotion” while the latter is referred to as “secular motion” [25].

The two kinds of motion have very different properties: most importantly, the frequency of the micromotion is typically high and, in particular, higher than the width of the dark resonances. As a result, micromotion generally leads to a frequency modulated spectrum, with the appearance of echos and with a corresponding reduction of the depth of these resonances without significant change in their width [26]. Secular motion, on the other hand, takes place at lower frequencies and results in a broadening of the dark resonances [22]. For simplicity, in the following we will neglect micromotion and focus on the spectral effect of the secular motion alone.

First, we will further simplify our calculation by assuming that the ion’s motion is one-dimensional, and later extend it to the 3-dimensional case. This approximation is equivalent to neglecting the motion in two of the trap directions, or to assuming that one of the trap axes coincides with the propagation direction of the laser fields used to obtain the CPT spectrum.

We will also restrict to the case where a semiclassical description of the secular motion is valid. Each instance of the experiment can be assumed to correspond to a situation where the atomic position is oscillating at the secular frequency ω and with a given amplitude A

$$x(t) = A \sin(\omega t + \varphi) \quad (2)$$

with φ a random phase. For our simulations, the motion of the ion will be included as an external harmonic driving at the secular frequency. Given that the position of the ion can be described as Eq. (2), the velocity is

$$v(t) = A\omega \cos(\omega t + \varphi). \quad (3)$$

For an ion moving at a given velocity, the Doppler effect causes an effective detuning for each laser-transition pair of

$$\delta_j(t) = \Delta_j - k_j v(t) = \Delta_j - k_j A\omega \cos(\omega t + \phi), \quad (4)$$

where, k_j is the wavenumber for each laser indicated by the subindex $j = 0, 2$, and where we take the sign convention for the detuning at rest $\Delta_j = \omega_j^{(l)} - \omega_j^{(0)}$ where $\omega_j^{(0)}$ is the atomic transition frequency and $\omega_j^{(l)}$ is the laser frequency. This shift in the effective detunings cause a corresponding shift in the spectral position of the the dark resonances, and will thus be the basis to infer a temperature from the spectrum.

Throughout the following sections we consider a thermal distribution, so that the kinetic energy of the particle is a random variable that follows a Maxwell-Boltzman distribution. In our semiclassical treatment of the motion, the amplitude A is related to the mechanical energy E by $E = m(A\omega)^2/2$. The spectrum corresponding to a given mechanical energy can be obtained averaging over φ , and the results corresponding to a thermal state are calculated averaging over E with a Boltzmann weight. We will neglect the back-action of the electronic degrees of freedom on the motion, corresponding to the momentum change upon absorption and emission of photons. This is a reasonable approximation within the semiclassical regime, where typical values of momentum are much larger than the recoil kick, so that the time scale of the atomic motion is fast compared with the time scale over which effects due to these kicks become observable.

C. Temperature estimation from dark-resonance spectra

As discussed before, the Doppler shifts associated with an atomic velocity v lead to a shift in the position of the dark resonance. Thermal motion in a trap does not correspond to a fixed shift, but rather to an oscillating shift which has to be averaged over several realizations. As a result, dark resonances are broadened and weakened by the motion. For high enough temperature, the resonances tend to disappear completely. For low temperatures, the effect of the motion tends to be masked by other effects, such as laser linewidth, power broadening, or off-resonant transitions. For intermediate scenarios, the analysis of the dark resonances allows for an estimation of the temperatures [22, 24]. However, the extraction of a temperature value from an atomic spectrum requires a theoretical model to map changes in the spectrum to changes in temperatures. One reliable method is to try

to fit the measured spectrum to the full model. This is a non-trivial step as a precise model has the drawback of being exceedingly time consuming and usually has many free parameters which make the fit impractical or unreliable. On the other hand, some approximations that render the numerical simulation much faster are not always valid or accurate.

To include the temperature of the ion in the numerical calculation of the spectrum we follow four different approaches. We compare the results of these different procedures and discuss the applicability of each method. In the next section we discuss each simulation strategy for the case of the three-level system and in the following one we generalize our results to the more complex eight-level system.

III. SPECTRUM OF A THREE-LEVEL SYSTEM

We first discuss the theoretical model of the electronic dynamics. We consider the system described in Fig.1, as detailed before. Under the rotating wave approximation, and in the rotating frame, the electronic dynamics is described by the Hamiltonian

$$H = \hbar \begin{pmatrix} \Delta_0 & \frac{\Omega_{10}}{2} & 0 \\ \frac{\Omega_{10}}{2} & 0 & \frac{\Omega_{12}}{2} \\ 0 & \frac{\Omega_{12}}{2} & \Delta_2 \end{pmatrix}. \quad (5)$$

written in the basis $\{|0\rangle, |1\rangle, |2\rangle\}$. Here Ω_{10} and Ω_{12} are the Rabi frequencies and Δ_0, Δ_2 the detunings of the fields driving the respective transitions.

To include spontaneous emission and laser imperfections, we add a dissipative Lindblad superoperator to the system's master equation for the density matrix of the system ρ

$$\frac{d\rho}{dt} = -\frac{i}{\hbar} [H, \rho] + \mathcal{L}\rho = \mathcal{M}\rho. \quad (6)$$

Here \mathcal{M} is the superoperator generating the complete, non-unitary evolution, with dissipative terms given by

$$\mathcal{L}\rho = \sum_{\alpha=l,d} \sum_{j=0,2} \frac{1}{2} [C_{\alpha j}\rho, C_{\alpha j}^\dagger] + \text{H.c.} \quad (7)$$

Here, $j = 0, 2$ indicates a given lower state, while d stands for “decay” and l for “linewidth”. The four jump operators $C_{\alpha j}$ are the following:

$$\begin{aligned} C_{dj} &= \sqrt{\Gamma_{dj}} |j\rangle \langle 1| \\ C_{lj} &= \sqrt{2\Gamma_{lj}} |j\rangle \langle j| \end{aligned} \quad (8)$$

with Γ_{dj} the spontaneous decay rate from the excited state to the lower level $|j\rangle$, and Γ_{lj} the dephasing rates due to the linewidths of the respective lasers.

The master equation can be solved to find the dynamics of the density matrix and the evolution of the ion's

fluorescence, which is proportional to the population of the excited state, ρ_{11} . The effect of the motion leads to an oscillating variation of the detunings resulting from the Doppler shift. In general, atomic motion can also modify the electronic state through a spatial dependence of the Rabi frequencies, an aspect which we will not include since we will assume that the laser field can be treated as a plane wave with constant amplitude and polarization.

A. Driven motion approximation

The most accurate and time-consuming method we consider, which we will use to benchmark the rest, consists of numerically implementing the Optical Bloch Simulations (OBS) for the time-dependent evolution of the electronic state. To calculate the fluorescence from the simulations, we introduce the oscillatory time dependence of the laser detunings, as given by Eq. (4), in the Hamiltonian of Eq. (6) and find the full density matrix as a function of time. For each value E of the mechanical energy, the fluorescence is proportional to the time average of the excited state population, $\overline{\rho_{11}}(E)$, after a sufficiently long waiting time so that the numerical solution is approximately stationary.

If one assumes that the ion is in a thermal state in the semiclassical regime, the fluorescence for each set of parameters can be calculated as the weighted average

$$\mathcal{F}(T) = F_0 Z^{-1} \int_0^\infty \overline{\rho_{11}}(E) e^{-E/k_B T} dE \quad (9)$$

with k_B the Boltzmann constant, Z the partition function and F_0 a constant that depends on the light collection efficiency. The desired spectrum is obtained by sweeping over Δ_2 while keeping Δ_0 fixed.

In figure 2 we show curves calculated by the driven motion approach, for $T = 20$ mK (black curve), two different trap frequencies ($\omega = 2\pi \times 0.1, 1$ MHz) and for a fixed set of laser intensities. The chosen parameters generate a dark resonance at $T = 0$ with a linewidth of ≈ 2 MHz, shown in the inset. For the higher temperature, we see that the resonance becomes broader and shallower and shifts to higher frequencies. Also, we observe that for the case when the trap frequency is lower than the zero-temperature linewidth, the spectrum appears smooth, while a non-smooth behavior with small fluctuations is observed at higher trap frequencies, i.e. when it is comparable to the electronic dynamics. In the following subsections we will discuss the different approximations and how well they reproduce these results.

As a reference of the computational resources needed for this method, we report the simulation time and system used. Simulating one of the curves by this method on one core of a Dell PowerEdge R720xd takes 20 minutes for a three-level system. On the other hand, for an eight-level system running on 32 cores, it takes over 20 hs for an eight-level system.

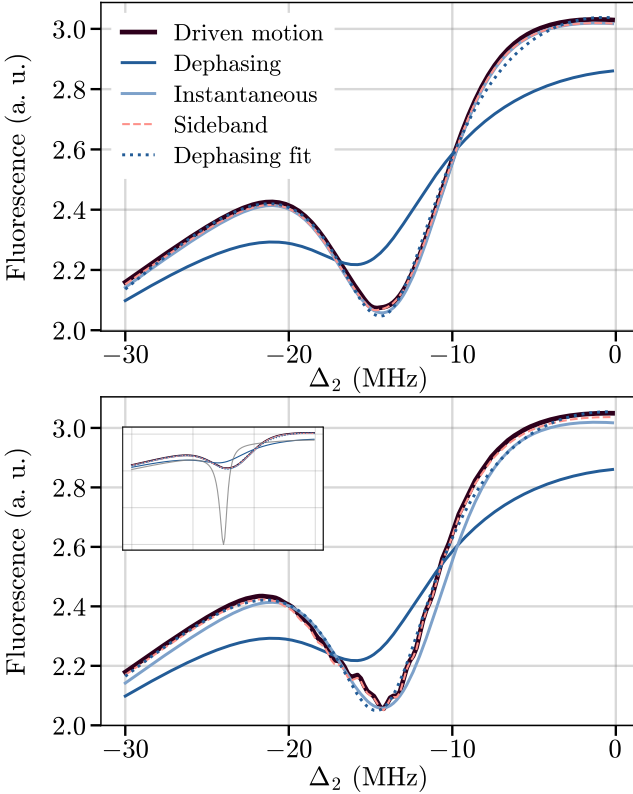


FIG. 2: Comparison of three-level spectra calculated with the four methods described, for $T = 20$ mK and assuming $^{40}\text{Ca}^+$ ions driven at the dipolar transition at 397 nm for doppler cooling and dipolar repump transition at 866 nm. In a) the trap frequency is $\omega = 2\pi \times 0.1$ MHz and in b) $\omega = 2\pi \times 1$ MHz. The dashed blue line is the spectra calculated by including thermal effects as dephasing, setting the temperature that yields the best fit ($T = 10.8$ mK in a), $T = 9.6$ mK in b)). We show plots for two different secular frequencies, assuming movement in one dimension. The inset shows the spectra of the main plot and the zero temperature spectrum for comparison.

B. Instantaneous relaxation approximation

The second method we consider is based on the assumption that the ion's motion is much slower than the characteristic relaxation time τ_r of the internal dynamics, as we detail below.

For each fixed value v of the velocity, i.e. with fixed Doppler-shifted detunings, we obtain the fluorescence as proportional to the steady-state population of the excited level with the replacement $\Delta_l \rightarrow \delta_l(v)$. We approximate the ion's external state as a classical thermal state, so that v is a random variable that follows a Maxwell-Boltzmann distribution, with temperature T . The total fluorescence as a function of the temperature and laser

detunings is approximated by

$$\mathcal{F}(T) = F_0 Z^{-1} \int \left(\frac{m}{2\pi k_B T} \right)^{1/2} \rho_{11}[\delta_0(v), \delta_2(v)] \times \exp \left[-\frac{1}{2} \left(\frac{v}{\sigma_T} \right)^2 \right] dv, \quad (10)$$

with $\sigma_T = \sqrt{k_B T / m}$ the thermal dispersion of the velocity, Z the partition function, and F_0 a factor that depends on the light collection efficiency. The resulting curve is plotted in figure 2 in light blue.

In practice, since the ion is trapped, its velocity will be oscillating and thus the previous expression will only be a good approximation as long as the velocity changes slowly enough with respect to the electronic dynamics. In fact, as seen in figure 2 in the light blue curve, this approximation holds well for the lower trap frequencies and shows some deviations from the previous results when the trap frequency is comparable to or larger than the dark resonance linewidth.

More precisely, we expect that Eq. (10) describes well the spectrum of an ion when the rate at which the equilibrium population of the excited state changes is significantly slower than the relaxation rate γ_r of the electronic dynamics at zero temperature. This can be expressed as the set of parameters for which the following inequality holds at all times

$$\gamma_r \gg \frac{1}{\rho_{11}} \frac{\partial \rho_{11}}{\partial t} = \frac{1}{\rho_{11}} \frac{\partial \rho_{11}}{\partial v} \frac{dv}{dt}. \quad (11)$$

Here, ρ_{11} is taken to be the asymptotic excited state population corresponding to a given instantaneous velocity v which in turn oscillates with the trap frequency.

Even for a simple 3-level system, calculating the condition (11) can be demanding. This is due to the presence of the dark resonance, which has an impact on both sides of the inequality: on the left, the relaxation rate will generally be much smaller than the scale of spontaneous decay from the excited level; on the right, the dependence of ρ_{11} on the instantaneous velocity will be sharper close to the resonance. The most straightforward method to check the condition (11) is to evaluate it numerically. In general, we find that the instantaneous approximation is not well justified for systems with pronounced dark resonances as discussed in Appendix B 2.

Finally, it is interesting to note that for the simpler case of a two-level dipole transition, the instantaneous approximation typically holds. This result is derived analytically in Appendix A.

C. Sidebands approximation

When the characteristic timescales of the external and internal dynamics are comparable, the instantaneous approximation breaks. In this regime, the electronic degrees

of freedom are influenced by the atomic velocity at earlier times. The time dependence of the motion can then be included in a Floquet-type expansion. Here we follow the approach originally introduced to describe micromotion echoes in a three and eight level system [27], but adapted to describe secular motion. This procedure is closely related to the calculations presented in [26, 28].

For each simulation run, we assume that the ion oscillates at the relevant secular frequency ω with an amplitude A as in Eq. (2). The superoperator \mathcal{M} generating the time evolution of the electronic degrees of freedom in Eq. (6) will then have time-dependent coefficients, i.e. $\mathcal{M} = \mathcal{M}_0 + 2\Delta\mathcal{M} \cos(\omega t)$, where $\Delta\mathcal{M}$ is proportional to the oscillation amplitude A . The equation for the steady state can be solved proposing solutions of the form

$$\rho(t) = \sum_{n=-\infty}^{\infty} \rho^{(n)} e^{in\omega t} \quad (12)$$

with components oscillating at all integer multiples of the driving frequency.

Since we are interested in experiments collecting light for time intervals typically longer than the period of the oscillation, we are only interested in the time-averaged density matrix, $\bar{\rho}$, which is equal to $\rho^{(0)}$. However, the evolution of each of the components is coupled with the rest. Indeed, replacing the expression above in the master equation (6) one obtains:

$$\sum_{n=-\infty}^{\infty} \rho^{(n)} n i \omega e^{in\omega t} = (\mathcal{M}_0 + 2\Delta\mathcal{M} \cos \omega t) \sum_{n=-\infty}^{\infty} \rho^{(n)} e^{in\omega t}. \quad (13)$$

From this equation a recurrence relation can be derived for $\rho^{(n)}$. In order to solve this relation and find the relevant contribution $\rho^{(0)}$ one resorts to a truncation [27]. This is justified because the amplitude of each sideband (labeled by n) scales approximately as the corresponding Bessel function evaluated in the modulation factor $J_n(kA)$, with k the largest wavevector. One can then truncate the expansion, setting to zero the terms above a certain n_{\max} of the order of kA , and recursively solve for $\rho^{(0)}$.

For each oscillation amplitude A , corresponding to a certain mechanical energy E , the total fluorescence is proportional to the time-averaged population of the excited state, $\bar{\rho}_{11}(E)$. The final spectrum for a thermal state is obtained by integrating contributions as in Eq. (9).

We find that in the one-dimensional case this approximation accurately captures the system's dynamics and reproduces all the key features of the full “driven-motion approximation” while significantly reducing computational cost. We run the model with 10 terms and obtain a spectrum in 18 seconds running on one core of a Dell PowerEdge R720xd processor. The results are plotted in figure 2 (pink), in complete agreement with the driven motion curve.

Unfortunately, the effectiveness of this method diminishes when the motion in three spatial dimensions is relevant, as it can only accurately account for one oscillating frequency. We will further discuss this in the following section for the eight-level system.

D. Effective dephasing approximation

The last method we consider is based on Ref. [22], where the temperature is added by introducing an effective thermal dephasing in the model. This approximation drastically reduces the computational cost of fitting experimental spectra, but yields results that are not properly calibrated to the real temperature. However, as we show here, the method can be calibrated to produce accurate results.

The strategy consists in accounting for the ion's motion through an effective dephasing of the electronic levels. This dephasing is chosen proportional to the Doppler broadening corresponding to a certain temperature T . Following [22], we focus on the Doppler broadening of the two-photon transition, since this process has the largest impact on the dark resonance. The effective dephasing rate depends on the relative modulus of the wave vectors $|\vec{k}_0 - \vec{k}_2|$ and the standard deviation of the corresponding thermal distribution

$$\Gamma_D \propto |\vec{k}_0 - \vec{k}_2| \sqrt{\frac{k_B T}{m}}. \quad (14)$$

Since one resorts to an effective dephasing associated with the difference between the two Doppler shifts, one must decide how to include it in (8). We add Γ_D to the dissipators corresponding to each of the linewidths as

$$\Gamma_{lj} \rightarrow \Gamma_{lj}^{(\text{eff})} = \sqrt{\Gamma_{lj}^2 + \Gamma_D^2 \frac{k_j^2}{k_0^2 + k_2^2}} \quad j = 0, 2, \quad (15)$$

i.e. weighing Γ_D by the ratio between wavevectors. In typical experiments the laser linewidths Γ_{lj} can be made small enough such that the above expressions are dominated by thermal effects, so that

$$\Gamma_{lj}^{(\text{eff})} \simeq \Gamma_D \frac{|k_j|}{\sqrt{k_0^2 + k_2^2}} \quad j = 0, 2. \quad (16)$$

We note that our particular choice of share of thermal dephasing to each laser does not have a significant impact on the depth or shape of the dark resonances. What is critical is the choice of the prefactor in the definition of Γ_D , Eq. (14). In [22] a prefactor of $1/\sqrt{2}$ was proposed. We find in our analysis that, when compared to the driven motion curves, the choice of this prefactor can underestimate or overestimate the temperature depending on the experimental parameters.

Two examples of overestimation can be seen in Fig. 2. In blue we show the spectra generated by setting the prefactor as $1/\sqrt{2}$ and the input temperature value, showing

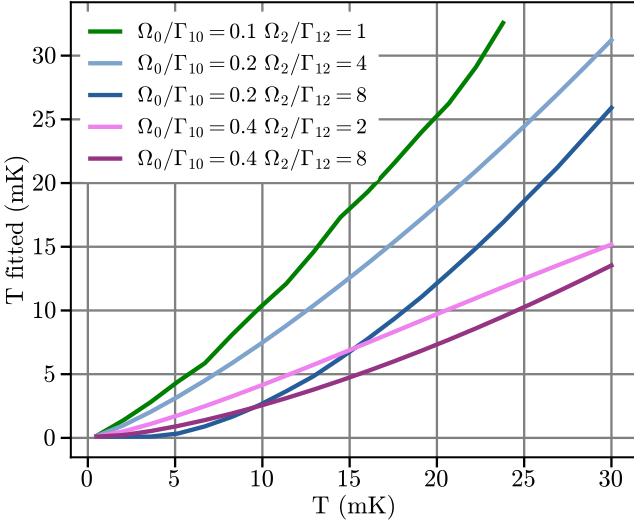


FIG. 3: Temperature resulting from a fit by the dephasing model as a function of the input temperature for the spectra generated by OBS, for different Rabi frequencies. Here we show results for a three-level system taking the decay rates so that they match those of $^{40}\text{Ca}^+$ ions, *i.e.* $\Gamma_{10} = 2\pi \times 21.58$ MHz and $\Gamma_{12} = 2\pi \times 1.35$ MHz [29].

no good agreement with the driven motion approximation. In blue dashed line we display the result from fitting the driven motion curve with the dephasing model taking the temperature as a free parameter. In this case the model reproduces the correct behavior but with a different value of the temperature.

To study this in detail, we fit the spectra generated from the time-dependent Bloch equations for various temperatures by the solution of (6) including thermal effects through dephasing. The temperature extracted from the best fit is plotted as a function of the input temperature for different Rabi frequencies in Fig. 3. The plot indicates that the approximation of thermal effects by effective dephasing as discussed above is particularly poor for temperatures below 10 mK, where the fit can underestimate the input temperature by an order of magnitude. Besides, the relation between the fit result and the input temperature depends on the Rabi frequency. Nevertheless, in principle, the effective dephasing technique can provide a good temperature estimate in cases where the approximate Rabi frequencies are known, allowing for a calibration of the fitted temperature. In the following section, we propose two paths for calibrating the effective dephasing fit, using the experimentally relevant eight-level system.

IV. EIGHT LEVEL SYSTEM

The three-level system analysis gives insight into how the presence of dark resonances changes the dynamics of

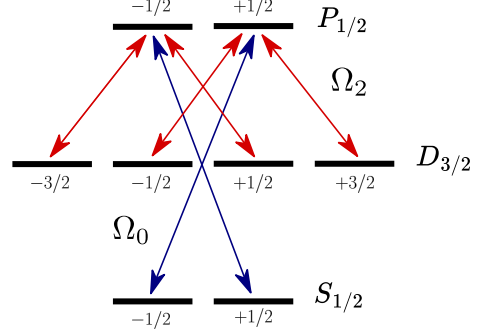


FIG. 4: Energy diagram of an eight-level system corresponding to the $^{40}\text{Ca}^+$ ion. It represents an ion with a Λ -type scheme. Under the effect of an external magnetic field, the Zeeman shift breaks the degeneracy within each level. The polarizations of the lasers determine the allowed transitions, marked by arrows in the diagram for the case when each of the lasers is linearly polarized in a direction orthogonal to the magnetic field.

the excited levels and how one can efficiently model the effect of the finite temperature of an ion. The characteristic relaxation rates are much smaller than in the case of a dipolar transition of a two-level system, which results in smaller regions of the space of parameters where the instantaneous approximation is valid. This becomes even more restrictive in the case of the eight-level system we now discuss. On the other hand, the sideband method takes into account the relaxation time, but strongly relies on the assumption that only one frequency of oscillation is relevant. The consequences of this approximation will be explored in the following.

We tackle a system corresponding to the eight-level model of $^{40}\text{Ca}^+$, whose energy diagram is sketched in Fig. 4. The ground S and excited P states are connected by a dipolar transition driven near 397 nm with Rabi frequency Ω_0 and the metastable D level is depopulated by driving the D - P transition near 866 nm with Rabi frequency Ω_2 . The decay rate from P to S , Γ_{10} , is set to $2\pi \times 21.58$ MHz, and the one from the P to the D manifold, Γ_{12} , to $2\pi \times 1.35$ MHz [29]. The ground S state and excited P state are doubly degenerate, while the metastable D level has four-fold degeneracy. In the presence of an external magnetic field, the Zeeman splittings break the degeneracy within each manifold. The Hamiltonian and dissipator of this eight-level system are described in detail in [22, 30].

Depending on the relation between the direction of the magnetic field and the polarization of the lasers, only some transitions are allowed. As in the three-level case, the formation of dark states leads to dark resonances in the spectrum. In this case, however, many more dark resonances may appear, corresponding to coherent superpositions of different sublevels of the S and D manifolds. The polarization of the lasers relative to the magnetic

field will determine the amount of dips that appear in the CPT spectra. We will study the case when each of the lasers is linearly polarized orthogonal to the magnetic field, exhibiting four dark resonances.

A. Comparison of simulation procedures

In Fig. 5 we show the spectra generated for the eight-level system using the different numerical approaches considered: the effective dephasing, the instantaneous approximation, the OBS with driven motion, and averaging over sidebands. Results are shown for $T = 10$ mK.

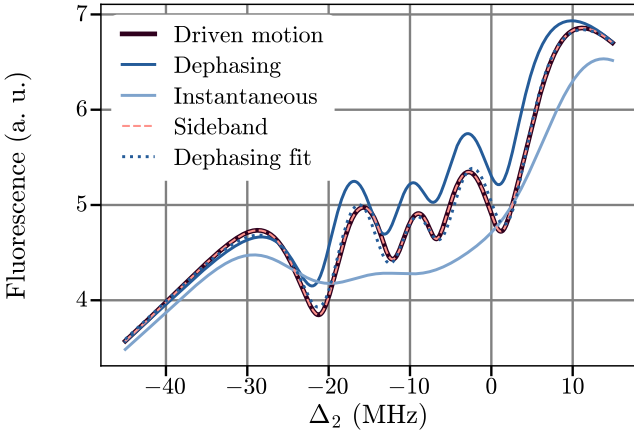


FIG. 5: Comparison of eight-level spectra calculated with different methods, for $T = 10$ mK and assuming $^{40}\text{Ca}^+$ ions. The curves from the sideband method are indistinguishable from the full OBS. The dashed line is the spectrum calculated by including thermal effects as dephasing, but for the temperature that yields the best fit. Rabi frequencies are $\Omega_0 = 0.4\Gamma_{10}$, $\Omega_2 = 8\Gamma_{12}$ and $T_{\text{fit}} = 5.7$ mK.

As with the three-level system, the temperature range within which the instantaneous approximation describes well the spectrum depends strongly on the parameters chosen. For the experimentally realistic parameters that we explore, the instantaneous approximation generally does not reproduce well the spectra, since it drastically suppresses the dark resonances.

Since the calculation of the spectra by averaging sidebands or using the full OBS has a high computational cost for an eight-level system and the instantaneous approximation is not applicable, it can be convenient to use the dephasing model to fit experimental data. Actually, as seen in Fig. 5, the comparison of the fit using the effective dephasing model (in dashed blue) with the more accurate calculation (in black) suggests that the dephasing method does resemble the true spectrum, but for a different temperature.

In Fig. 6, we compare the temperature that gives the best fit using the dephasing model with the input temperature for the spectrum calculated using sidebands, for

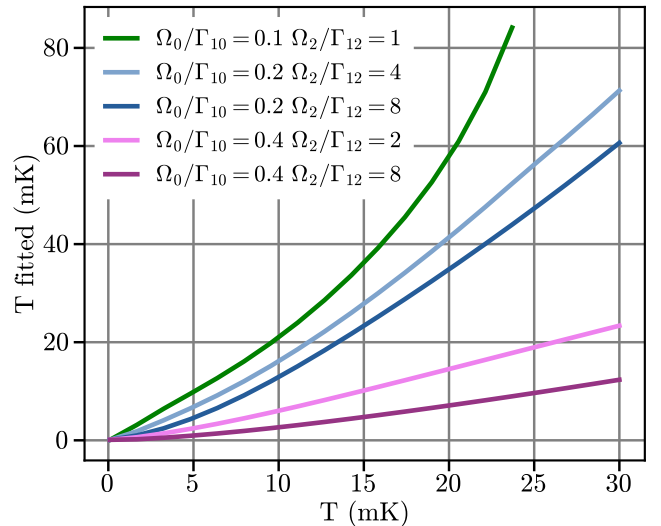


FIG. 6: Temperature resulting from a fit by the dephasing model as a function of the input temperature for the spectra generated by OBS with driven motion, for different Rabi frequencies. Here we show the results for the eight-level system corresponding to $^{40}\text{Ca}^+$ ions as described in the main text.

different choices of the Rabi frequencies. We find that, keeping all other input parameters fixed, the relation between both temperatures is monotonic but not always linear. We note that to properly fit the spectra, the Rabi frequencies must be left as free parameters of the dephasing model.

With a proper estimation of the Rabi frequencies, the use of the dephasing model to measure temperatures from fits of the spectrum can be practical and convenient. A possible route to extract the Rabi frequencies is to fit a spectrum from a cold ion, near 1 mK for instance, such that thermal effects are negligible. With this information one can choose the appropriate calibration curve.

B. Spectrum of an ion moving in three dimensions

The results so far suggest that one can perform the calibration of the spectra from the simulation with the sideband method, which is computationally less demanding than the solution of the OBS with driven motion. However, we have assumed that the Doppler shift could be described as a harmonic oscillation with a single frequency, which corresponds to the case when the propagation direction of both lasers coincides with one trap axis. When more motional frequencies are present, the sideband method cannot include them all, as it is based on a recursive solution with a single frequency.

One can still approximate the spectrum of an ion moving in three directions by the sideband method considering only motion along one trap axis. To choose this

axis, we take the direction with the largest projection of the driving lasers, which we assume to be collinear. As can be seen in Fig. 7 a), when the effective wavevector has a comparable projection onto different axes of the trap, the sideband approximation deviates slightly from the full model. However, as expected, if one assumes the projection of the lasers is much larger in one of the directions of the trap, the two spectra become more similar, as shown in Fig. 7 b).

Depending on the configuration of the lasers with respect to the trap, the sideband approximation can be more or less reliable to calibrate the temperature of the ion. As an example, in Fig. 7 a) the fit of the full driven motion curve for $T = 10$ mK by the dephasing model corresponds to a fit temperature of 3.4 mK whereas fitting the spectrum produced by the sideband approximation with only one of the frequencies and $T = 10$ mK yields a fit of 4.7 mK. In contrast, for the case of Fig. 7 b) where the projection of the laser is mainly along the z trap axis the values from the fits are $T = 4.6$ mK and $T = 4.7$ mK respectively, so that the calibration becomes more accurate.

Further numerical checks indicate that the error introduced by using the sideband approximation neglecting two of the motional frequencies decreases as the Rabi frequencies increase.

V. CONCLUSIONS

In this work we studied how to estimate the temperature of a single ion through dark-resonance spectra using different numerical methods. The most precise techniques we evaluate are computationally very costly, while the more efficient ones produce inaccurate results. However, we show that these faster methods can be properly calibrated, yielding a beneficial combination of precision and computational economy.

Of particular interest for our purposes was the method of replacing thermal motion by an effective dephasing due to Doppler broadening. This procedure is computationally inexpensive while still reproducing important spectral features. Indeed, this idea has been used in several articles to obtain fits of the spectrum in order to estimate the temperature. We note, however, that depending on the parameter regime of interest, this kind of fit can give temperature estimates that are off by up to an order of magnitude. Nonetheless, we described how this issue can be counteracted with a careful calibration of the experiment.

Our analysis focused on temperatures of the order of tens of millikelvin, a regime in which the motion of the ion can be treated by means of semiclassical approximations. This choice is related to the longer-term goal of performing reliable simulations of vibrational energy transport,

thermalization, and non-equilibrium thermodynamics in ion traps.

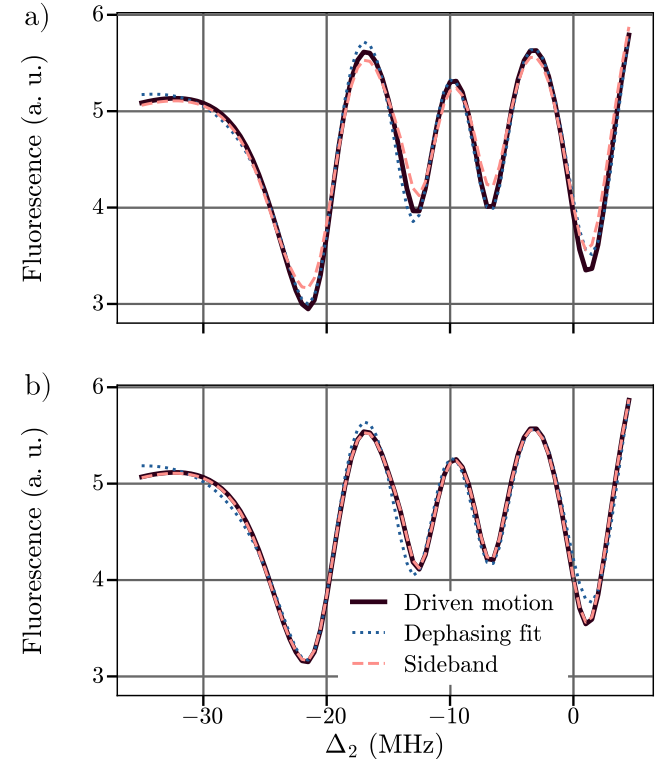


FIG. 7: a) CPT spectrum generated by the driven motion approximation with three dimensional movement and the lasers wavevectors relative to the trap's axes $\hat{k} \propto (1, 1, 2)$. Also shown are the spectrum generated by the sidebands approximation, and the fit by the dephasing model of both curves. b) shows the same but with the lasers wavevectors $\hat{k} \propto (1, 1, 8)$. For the curves in a), the estimated temperatures are $T_{\text{fit}} = 4.7$ mK and $T_{\text{fit}} = 3.4$ mK for the Sideband and driven motion approximations, respectively. For b), the fitted temperature for the driven motion curve is $T_{\text{fit}} = 4.6$ mK. The parameters are, for both figures, $\omega_x = 2\pi \times 0.6$ MHz, $\omega_y = 2\pi \times 0.8$ MHz $\omega_z = 2\pi \times 1.2$ MHz; $T = 10$ mK; $\Omega_0 = 0.4\Gamma_{10}$, $\Omega_2 = 8\Gamma_{12}$, $\Delta_0 = -2\pi \times 15$ MHz.

ACKNOWLEDGEMENTS

This work was supported by Agencia I+D+i grants PICT2018-3350, PICT2019-4349, PICT 2020-SERIEA-00959 and PICT 2021-I-A-01288, and Universidad de Buenos Aires grant UBACyT2023-20020220400119BA. The computational resources used in this work were provided (in part) by the HPC center DIRAC, funded by Instituto de Fisica de Buenos Aires (UBA-CONICET) and part of SNCAD-MinCyT initiative, Argentina.

[1] N. Freitas, E. A. Martinez, and J. P. Paz, Heat transport through ion crystals, *Physica Scripta* **91**, 013007 (2015).

[2] A. Bermudez, M. Bruderer, and M. B. Plenio, Controlling and measuring quantum transport of heat in trapped-ion crystals, *Phys. Rev. Lett.* **111**, 040601 (2013).

[3] A. Ruiz, D. Alonso, M. B. Plenio, and A. del Campo, Tuning heat transport in trapped-ion chains across a structural phase transition, *Phys. Rev. B* **89**, 214305 (2014).

[4] A. Ruiz-García, J. J. Fernández, and D. Alonso, Delocalization and heat transport in multidimensional trapped ion systems, *Phys. Rev. E* **99**, 062105 (2019).

[5] L. Timm, H. Weimer, L. Santos, and T. E. Mehlstäubler, Heat transport in an ion coulomb crystal with a topological defect, *Phys. Rev. B* **108**, 134302 (2023).

[6] M. Ramm, T. Pruttivarasin, and H. Häffner, Energy transport in trapped ion chains, *New Journal of Physics* **16**, 063062 (2014).

[7] O. Onishchenko, G. Guarnieri, P. Rosillo-Rodes, D. Pijn, J. Hilder, U. G. Poschinger, M. Perarnau-Llobet, J. Eisert, and F. Schmidt-Kaler, Probing coherent quantum thermodynamics using a trapped ion, *Nature Communications* **15**, 10.1038/s41467-024-51263-3 (2024).

[8] Z. Meir, M. Pinkas, T. Sikorsky, R. Ben-shlomi, N. Akerman, and R. Ozeri, Direct observation of atom-ion nonequilibrium sympathetic cooling, *Physical Review Letters* **121**, 10.1103/physrevlett.121.053402 (2018).

[9] D. Von Lindenfels, O. Gräß, C. T. Schmiegelow, V. Kaushal, J. Schulz, M. T. Mitchison, J. Goold, F. Schmidt-Kaler, and U. G. Poschinger, Spin heat engine coupled to a harmonic-oscillator flywheel, *Physical review letters* **123**, 080602 (2019).

[10] J. Roßnagel, O. Abah, F. Schmidt-Kaler, K. Singer, and E. Lutz, Nanoscale heat engine beyond the carnot limit, *Phys. Rev. Lett.* **112**, 030602 (2014).

[11] W. Neuhauser, M. Hohenstatt, P. E. Toschek, and H. Dehmelt, Localized visible ba^+ mono-ion oscillator, *Phys. Rev. A* **22**, 1137 (1980).

[12] B. G. Norton, E. W. Streed, M. J. Petrasius, A. Jechow, and D. Kielpinski, Millikelvin spatial thermometry of trapped ions, *New Journal of Physics* **13**, 113022 (2011).

[13] I. A. Boldin, A. Kraft, and C. Wunderlich, Measuring anomalous heating in a planar ion trap with variable ion-surface separation, *Phys. Rev. Lett.* **120**, 023201 (2018).

[14] Z.-C. Mao, Y.-Z. Xu, Q.-X. Mei, W.-D. Zhao, Y. Jiang, Z.-J. Cheng, X.-Y. Chang, L. He, L. Yao, Z.-C. Zhou, Y.-K. Wu, and L.-M. Duan, Observation of anomalous heat transport in a trapped ion chain, *Phys. Rev. A* **105**, 033107 (2022).

[15] D. J. Wineland, R. E. Drullinger, and F. L. Walls, Radiation-pressure cooling of bound resonant absorbers, *Phys. Rev. Lett.* **40**, 1639 (1978).

[16] J. H. Wesenberg, R. J. Epstein, D. Leibfried, R. B. Blakestad, J. Britton, J. P. Home, W. M. Itano, J. D. Jost, E. Knill, C. Langer, R. Ozeri, S. Seidelin, and D. J. Wineland, Fluorescence during doppler cooling of a single trapped atom, *Phys. Rev. A* **76**, 053416 (2007).

[17] R. J. Epstein, S. Seidelin, D. Leibfried, J. H. Wesenberg, J. J. Bollinger, J. M. Amini, R. B. Blakestad, J. Britton, J. P. Home, W. M. Itano, J. D. Jost, E. Knill, C. Langer, R. Ozeri, N. Shiga, and D. J. Wineland, Simplified motional heating rate measurements of trapped ions, *Phys. Rev. A* **76**, 033411 (2007).

[18] D. J. Wineland, W. M. Itano, J. C. Bergquist, and R. G. Hulet, Laser-cooling limits and single-ion spectroscopy, *Phys. Rev. A* **36**, 2220 (1987).

[19] C. Monroe, D. M. Meekhof, B. E. King, S. R. Jefferts, W. M. Itano, D. J. Wineland, and P. Gould, Resolved-sideband raman cooling of a bound atom to the 3d zero-point energy, *Phys. Rev. Lett.* **75**, 4011 (1995).

[20] P. A. Ivanov, Quantum thermometry with trapped ions, *Optics Communications* **436**, 101 (2019).

[21] I. Vybornyi, L. S. Dreissen, D. Kiesenhofer, H. Hainzer, M. Bock, T. Ollikainen, D. Vadlejch, C. F. Roos, T. E. Mehlstäubler, and K. Hammerer, Sideband thermometry of ion crystals, *PRX Quantum* **4**, 040346 (2023).

[22] J. Roßnagel, K. N. Tolazzi, F. Schmidt-Kaler, and K. Singer, Fast thermometry for trapped ions using dark resonances, *New Journal of Physics* **17**, 045004 (2015).

[23] T. Peters, B. Wittrock, F. Blatt, T. Halfmann, and L. P. Yatsenko, Thermometry of ultracold atoms by electromagnetically induced transparency, *Phys. Rev. A* **85**, 063416 (2012).

[24] V. Tugayé, J.-P. Likforman, S. Guibal, and L. Guidoni, Absolute single-ion thermometry, *Phys. Rev. A* **99**, 023412 (2019).

[25] D. Leibfried, R. Blatt, C. Monroe, and D. Wineland, Quantum dynamics of single trapped ions, *Reviews of Modern Physics* **75**, 281 (2003).

[26] N. A. Nuñez Barreto, M. Bonetto, M. A. Luda, C. Cormick, and C. T. Schmiegelow, Dark resonance spectra of trapped ions under the influence of micromotion, *Frontiers in Quantum Science and Technology* **3**, 1381117 (2024).

[27] H. Oberst, *Resonance fluorescence of single barium ions* (master's thesis, 1999).

[28] T. Sikorsky, Z. Meir, N. Akerman, R. Ben-shlomi, and R. Ozeri, Doppler cooling thermometry of a multilevel ion in the presence of micromotion, *Physical Review A* **96**, 10.1103/physreva.96.012519 (2017).

[29] M. Hettrich, T. Ruster, H. Kaufmann, C. F. Roos, C. T. Schmiegelow, F. Schmidt-Kaler, and U. G. Poschinger, Measurement of dipole matrix elements with a single trapped ion, *Phys. Rev. Lett.* **115**, 143003 (2015).

[30] N. A. Nuñez Barreto, M. Drechsler, and C. T. Schmiegelow, Three-laser coherent population trapping in a multi- Λ system: Theory, experiment, and applications, *Physical Review A* **106**, 10.1103/physreva.106.053708 (2022).

[31] W. Demtroder, *Laser spectroscopy* (Springer, Berlin, Germany, 2002) pp. 71–72, 3rd ed.

Appendix A: Spectrum of a two-level system

In order to better understand the effect of thermal motion on the fluorescence spectrum, we will also study the simplest possible model, i.e. the two-level atom. We consider only two electronic levels of an atom at rest, with a monochromatic wave driving the transition from the

ground state $|0\rangle$ to the excited state $|1\rangle$. Under the rotating wave approximation and in the rotating frame, the dynamics is described by the Hamiltonian

$$\hat{\mathcal{H}} = \hbar \begin{pmatrix} \Delta & \frac{\Omega}{2} \\ \frac{\Omega}{2} & 0 \end{pmatrix}. \quad (\text{A1})$$

where Ω is the Rabi frequency and Δ the detuning of the drive to the transition, with the sign convention $\Delta = \omega_l - \omega_0$ where ω_0 is the atomic transition frequency and ω_l is the laser frequency. The Hamiltonian above is written in the basis $\{|0\rangle, |1\rangle\}$ with $|0\rangle$ the ground state and $|1\rangle$ the excited level. The system's master equation is:

$$\frac{d\rho}{dt} = M\rho = i [\hat{\mathcal{H}}, \rho] + \mathcal{L}_{\text{damp}}(\rho) \quad (\text{A2})$$

where M is a superoperator with

$$\begin{aligned} \mathcal{L}_{\text{damp}}(\rho) &= -\frac{1}{2} [\hat{C}^\dagger \hat{C} \rho + \rho \hat{C}^\dagger \hat{C} - 2\hat{C}\rho\hat{C}^\dagger] \\ \hat{C} &= \sqrt{\Gamma} |0\rangle \langle 1|, \end{aligned} \quad (\text{A3})$$

where Γ is the rate of spontaneous decay. We do not include here dephasing due to laser frequency fluctuations since they have a negligible impact in this system; this need not be the case for models including more electronic levels.

The stationary solution when the ion is at rest has an analytical expression,

$$\rho_{11} = \frac{\Omega^2}{\Gamma^2 + 4\Delta^2 + 2\Omega^2}. \quad (\text{A4})$$

To include the temperature of the ion in the model we follow the same four different approaches as with the three- and eight-level systems. The validity of the approximations for this system differs from the more complex ones, since the absence of dark resonances means that the characteristic time scale of the system is, at least, the decay rate of the corresponding dipolar transition. As in the main text, we take the driven motion approximation as a benchmark.

The comparison of the four methods described in the main text for a two-level system can be seen in Fig. 8, for different values of the ratio Ω/Γ , and taking $\Gamma = 2\pi \times 21.58$ MHz. We note that choosing a different value of Γ is equivalent to rescaling temperature accordingly, given the very few parameters in this simplified model. The results from driven motion and instantaneous approximation are indistinguishable for the parameter ranges in the figure, which correspond to typical experimental values. The sidebands approach is a very good approximation as long as one sums over enough sidebands. In our case, we find that by taking $n_{\text{max}} = kA$, the method gives a good result. On the contrary, the effective dephasing leads to a much worse approximation of the spectrum. We note, however, that all curves become very similar for lower temperatures.

Appendix B: Instantaneous relaxation approximation

1. Two-level system

The instantaneous relaxation approximation is as before, only now the population of the excited level is as

A4

$$\mathcal{F}(T, \Delta) \propto \int \left(\frac{m}{2\pi k_B T} \right)^{1/2} \rho_{11}(\Delta - kv) e^{-\frac{1}{2} \left(\frac{v}{\sigma_T} \right)^2} dv, \quad (\text{B1})$$

where

$$\sigma_T = \sqrt{\frac{k_B T}{m}}. \quad (\text{B2})$$

The shape of this absorption spectra is called a Voigt profile [31], the convolution of a Lorentzian profile and a Gaussian probability density.

This result will only be a good approximation as long as velocity changes slowly enough. More precisely, we expect that Eq. (B1) describes well the spectrum of an ion when the following inequality holds at all times:

$$\frac{1}{\rho_{11}} \frac{\partial \rho_{11}}{\partial t} \sim \frac{1}{\rho_{11}} \frac{\partial \rho_{11}}{\partial v} \omega v \sim \frac{8kv\omega\delta}{\Gamma^2 + 2\Omega^2 + 4\delta^2} \ll \frac{\Gamma}{2} \quad (\text{B3})$$

where ρ_{11} is taken to be the asymptotic excited state population corresponding to a given instantaneous velocity v which in turn oscillates with the trap frequency. For values of detuning of the order of Γ , we have

$$kv \ll \frac{5\Gamma^2}{16\omega}. \quad (\text{B4})$$

This relation takes a more complicated, but less restrictive form for smaller absolute values of the detuning.

For $^{40}\text{Ca}^+$ ions, the dipole transition used for Doppler cooling and fluorescence detection has a natural linewidth given by $\Gamma \approx 2\pi \times 21.58$ MHz. Considering typical trap frequencies, for temperatures below 100 mK the condition above is usually fulfilled and the instantaneous approximation is expected to hold.

2. Three-level system

The relaxation rate γ_r is calculated as the absolute value of the smallest real part of the non-zero eigenvalues of the superoperator \mathcal{M} generating the evolution. In figure Fig. 9 we show the quotient between both sides of Eq (11) for different Rabi frequencies. For small secular frequencies, the inequality holds under an order of magnitude for all laser intensities studied. As the frequency increases, the inequality turns and the instantaneous approximation becomes less accurate relative to our benchmark. Furthermore, the frequency for which it no longer holds depends on the laser intensity. This is consistent with what we discussed earlier, that as the dark resonance broadens, the rate of relaxation increases, analogously to a dipolar transition.

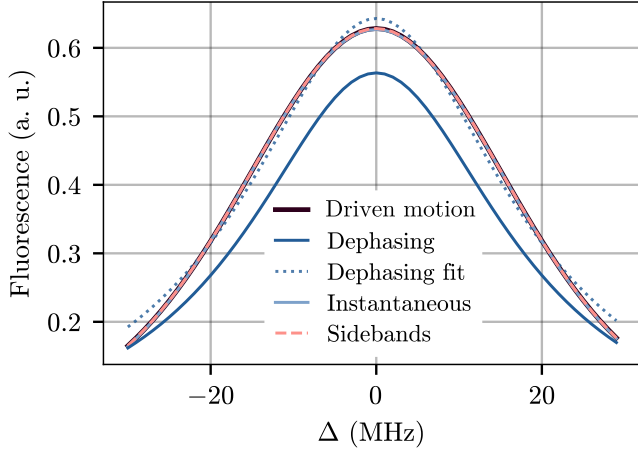
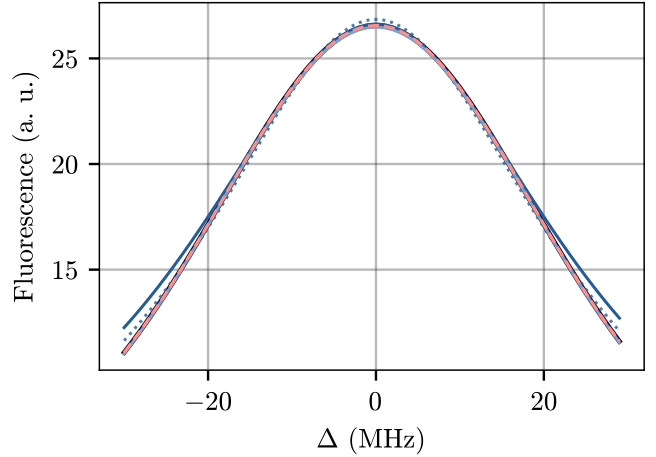
(a) $\Omega/\Gamma = 0.1$ (b) $\Omega/\Gamma = 1$

FIG. 8: Comparison of two-level spectra calculated with the four methods described, for $T = 100$ mK and assuming $^{40}\text{Ca}^+$ ions driven at the dipolar transition at 397 nm. The Instantaneous, Sidebands and OBS with driven motion curves are overlapped. The pointed line is the spectra calculated by including thermal effects as dephasing, setting the temperature that yields the best fit.

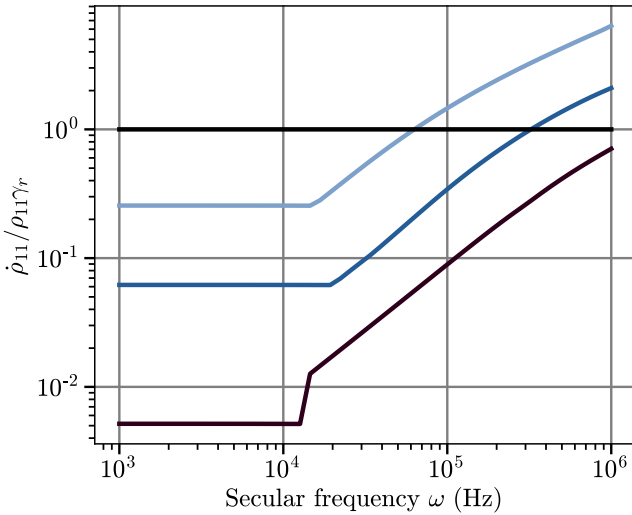


FIG. 9: Relative time derivative of the excited level population divided by the relaxation rate as a function of the frequency ω of the thermal motion. We show three cases with increasing laser intensities: $\Omega_0/\Gamma_{01} = \{0.1, 0.3, 0.5\}$ and $\Omega_2/\Gamma_{12} = \{1, 3, 6\}$ in colors {light blue, blue, purple}, correspondingly. For all plots, $\Delta_0 = -2\pi \times 15$ MHz, $v = 2\sigma_T$ with $T = 20$ mK.